Iterative Cancellation of Multi-User Non-Aligned Inter Spreading Factor Interference in LoRa Systems

Qiaohan Zhang, Jia Zhang, Ana Belen Martinez, Ivo Bizon, Philipp Schulz and Gerhard Fettweis
Vodafone Chair for Mobile Communications Systems, Technische Universität Dresden, Germany.
Email: {qiaohan.zhang, jia.zhang, ana_belen.martinez_monton, ivo.bizon, philipp.schulz2, gerhard.fettweis}@tu-dresden.de

***Abstract*—Long Range (LoRa) technology has emerged as a promising communication solution for low power wide area networks. However, its ALOHA-based medium access scheme is prone to collisions, leading to limited network scalability. In congested LoRa networks, simultaneous transmission by multiple users using different spreading factors (SFs) results in inter-SF multi-user interference (MUI), thereby increasing packet loss likelihood under low signal-to-interference ratio (SIR) conditions. In this paper, we show the impact of MUI and propose an iterative interference cancellation method based on signal segmentation to address this issue. Our approach incorporates an algorithm for detecting MUI, which effectively identifies multiple interference SFs without prior knowledge, enabling interference cancellation without synchronizing interfering signals. Our numerical analysis demonstrates that MUI significantly impacts LoRa performance, but the proposed interference cancellation method can significantly reduce the symbol error rate under low SIR conditions compared to conventional demodulation. Our work makes a contribution to the field of LoRa technology, offering a practical and effective solution to the challenges posed by MUI in congested networks.**

***Index Terms*—Interference cancellation, Internet of Things (IoT), Long Range (LoRa), medium access, spreading factor.**

I. Introduction

Over the past few years, there has been significant interest in Internet of Things (IoT) wireless communications. Reliable data transmission over long distances with low power consumption is a critical requirement for IoT applications, such as remote sensing, soil monitoring, and weather forecasting, where IoT devices gather data from fields and transmit it to a centralized hub for analysis [1]. To address these requirements, low power wide area networks (LPWAN) have been specifically designed to provide adequate coverage and low power consumption. Among the leading LPWAN physical layer technologies, Long-Range (LoRa) has emerged as one of the most popular options, as it allows data transmission over long distances with low power consumption [2].

LoRa is a radio frequency modulation technology developed by Semtech that uses chirp spread spectrum (CSS) modulation for encoding data. This allows LoRa to transmit data over long distances while consuming very little power. LoRa's physical layer (PHY) utilizes the initial frequencies of chirp signals to differentiate LoRa symbols, enabling reliable transmission even in noisy environments [3], [4]. LoRa's PHY standard uses spreading factors (SFs) to determine the number of bits used to encode a LoRa symbol, which ranges from 7 to 12 bits. Smaller SFs are adopted for communication with higher data rates but shorter range, whereas larger SFs are capable of communication with longer range but reduced data rates. Signals modulated with different SFs present negligible but nonzero correlation, which is referred to as quasi-orthogonality [5]. Under this assumption, by changing the SF, a LoRa transmission channel can be further divided into independent subsystems without interfering with each other. However, in densely populated LoRa networks, simultaneous transmission of data by multiple users is common due to the ALOHA-based medium access scheme, and when users with different SFs transmit at the same frequency and time, the near-far problem can arise. This situation is characterized by the desired signal being transmitted from a farther source, while the undesired signals originate from nearby sources, resulting in the power of the desired signal being significantly lower than that of the undesired signals at the receiver end. In such situations, the correlation between signals with different SFs becomes non-negligible, and the orthogonality assumption no longer holds, thereby limiting the scalability of LoRa networks. The undesired signals from multiple users, which are superimposed on the desired signal in a random fashion, are referred to as multi-user inter-SF interference (MUI). This interference disrupts the demodulation process and complicates the reliable reception of LoRa signals.

Despite extensive research on interference in LoRa networks, the issue of inter-SF collision has received limited attention. Previous studies focused primarily on interference with the same SF, where users with identical SF transmit on the same frequency band and are subject to collisions [6], [7], [8], since the most significant collision occurs when the SFs are identical. The authors in [9] pointed out the non-negligible influence resulted from inter-SF collision, quantifying the signal-to-interference ratio (SIR) threshold required for rejecting the inter-SF interference. They show that under same-SF interference, collisions often result in demodulation of the strongest signal. In contrast, inter-SF interference has an impact on LoRa performance resembling white noise. Furthermore, the performance of successive interference cancellation (SIC) of the same-SF interference is also considerably degraded by inter-SF collisions in nodes far away from the base station [10]. The study in [11] shows that higher SFs are more vulnerable to inter-SF collision in spite of the employment of power control and packet fragmentation.

Mitigating the degradation caused by inter-SF collisions remains an unsolved problem that demands further investigation.The authors in [12] design a scheduler, named X-MAC, that is aware of the imperfect orthogonality between SFs. It is capable of detecting inter-SF collisions by tracking historical transmissions and enabling collision avoidance by performing dynamic channel scheduling. This scheme evaluates the status of packet loss and reschedules the channel to avoid collision. However, the inter-SF interference cannot be canceled from the historical signal, thus resulting in decoding mistakes. In [13], a friendly jamming scheme is proposed based on the inter-SF interference property. This scheme generates friendly jamming signals using a different SF to collide with non-friendly jamming signals. As a result, the demodulation of desired LoRa signals at the receiver is not affected by the attacker, since the inter-SF friendly jamming signals can be recovered and canceled at the receiving gateway. However, the preambles of the inter-SF interference need to be detected and synchronization is required. This becomes more challenging for random MUI, since the received signals may not include the preambles of the interference or the preamble structure may be unknown for synchronization. An approach for canceling inter-SF interference without synchronizing the interference signal was proposed in our previous work [14], where the interference signal can be reconstructed and eliminated concurrently using signal segmentation based on the CSS characteristics. Although this method yields promising outcomes, it is constrained to single-user inter-SF interference (SUI), and it is not capable to confirm the existence of multiple sources of interference. As such, the scheme can identify only one interfering SF without confirmation of its presence. LoRa networks with high device densities are better represented by the MUI model, which has been previously analyzed in [15].

This paper presents an iterative interference cancellation scheme to overcome the limitations imposed by MUI in LoRa networks. By estimating and reconstructing non-aligned MUI, the LoRa receiver enables iterative interference cancellation at the gateway. The main contributions of this paper are as follows.

- The MUI scenario is numerically modeled and analyzed, demonstrating that interference from multiple users with different SFs can lead to packet loss. In addition, the LoRa performance of MUI and SUI is compared.
- An algorithm is proposed to detect MUI, enabling iterative cancellation of interference. This approach extends our initial interference cancellation scheme presented in [14].
- We demonstrate that the proposed scheme is able to identify the SFs of MUI and the demodulation performance is significantly improved after MUI cancellation.

The structure of this paper is as follows. Section II presents an overview of the system model of LoRa, including an explanation of the CSS modulation mechanism. Section III discusses the impact of MUI. Section IV outlines the proposed iterative MUI cancellation scheme step by step. Section V demonstrates the simulation results of the proposed method. Finally, Section VI concludes the paper.

II. System Model

In LoRa, CSS modulation is implemented using the initial frequencies of chirp signals to encode information from data symbols [16]. The symbol energy is spread across a wider range of frequencies to increase the receiver sensitivity. This spreading of the symbol energy in frequency is achieved by varying the frequency of the chirp signal over time. In this paper, we follow the system model presented in [14], where a LoRa receiver samples the incoming signals at the Nyquist frequency. The equivalent equation of a discrete LoRa signal in the PHY can be described by:

$$x_k[n] = A_u \exp\left(j\frac{2\pi}{N_u}kn\right)c[n], \tag{1}$$

where SF_u is the SF of the desired user, $N_u = 2^{\mathrm{SF}_u}$ is the total number of samples within one LoRa signal, $A_u = \sqrt{E_s/N_u}$ is the signal amplitude, where E_s is the symbol energy, and n is the sample index. The data symbol k modulates the frequency of a complex exponential and its energy is spread by multiplication with a raw up-chirp in discrete time domain $c[n] = \exp\left(j\pi n^2/N_u\right)$. The values of k are restricted to integers within the set $\mathbb{K} = \left\{0, \ldots, 2^{\mathrm{SF}_u} - 1\right\}$. Every group of SF_u bits is mapped onto one symbol k, feeding the CSS modulator to generate LoRa signals.

Based on the model containing only SUI [14], we further extend to a more general case in which MUI exists on the same bandwidth as the desired user. Assuming that the receiver is perfectly synchronized with the desired signal, a data symbol interfered with data symbols from multiple users modulated with different SFs at the gateway can be described by

$$y_k[n] = h_u x_k[n] + \sum_{\beta=1}^{N_{\mathrm{MUI}}} h_{(\beta)} i_{(\beta)}[n] + w\,[n]\,, \tag{2}$$

where N_{MUI} is the total number of interferers and $i_{(\beta)}[n]$ represents the overlapped interference signal of the β-th interferer modulated with $\mathrm{SF}_{(\beta)}$ without synchronization, which also includes N_u samples. Since $\mathrm{SF}_u \neq \mathrm{SF}_{(\beta)}$, one desired data symbol can overlap multiple interference data symbols in the time domain or vice versa. h_u and $h_{(\beta)}$ are the complex-valued channel gains experienced by the desired user and the β-th interferer, respectively. $w[n] \sim \mathcal{CN}(0, \sigma^2)$ is additive white Gaussian noise (AWGN). It is necessary to note that (2) describes the collision period of one desired data symbol. The more complete expression of $i_{(\beta)}[n]$ in terms of the sample can refer to the description of SUI in [14].

In order to demodulate a LoRa signal, the conventional approach involves performing two steps within N_u samples, which comprise one data symbol. First, the received signal $y_k[n]$ is multiplied by the down chirp $c^*[n]$ for de-chirping as follows

$$r[n] = y_k[n]\exp\left(-j\pi n^2/N_u\right). \tag{3}$$

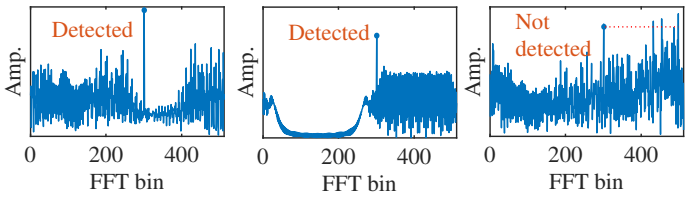

(a) SUI scenario with $\mathrm{SF}_{(1)} = 7$.

(b) SUI scenario with $\mathrm{SF}_{(2)} = 8$.

(c) MUI scenario with $\mathrm{SF}_{(1)} = 7$ and $\mathrm{SF}_{(2)} = 8$.

Fig. 1: FFT of different inter-SF scenarios with $\mathrm{SF}_u = 9$.

Then, the non-coherent detection in LoRa is performed by measuring the power of the received signal in the frequency domain, which enables the demodulation without compensation of the channel phase rotation. Thus, by selecting the maximum peak location in the frequency domain to obtain the data symbol, this operation can be described as

$$\hat{k} = \arg\max_{f \in \mathbb{K}} \left| R[f] \right|, \tag{4}$$

where $R[f] = \mathcal{F}\{r[n]\}$, and $\mathcal{F}\{\cdot\}$ represents the operation of discrete Fourier transform (DFT) of N_u points, which can be implemented using the fast Fourier transform (FFT) algorithm.

III. Impact of MUI

In the context of a LoRa network with multiple interferers, where interference signals are modulated with SFs different from the desired user, we define the SIR as follows:

$$\mathrm{SIR} = 10 \log_{10} \left(\frac{\mathcal{P}_u}{\sum_{\beta=1}^{N_{\mathrm{MUI}}} \mathcal{P}_{(\beta)}} \right), \tag{5}$$

where $\mathcal{P}_u$ and $\mathcal{P}_{(\beta)}$ are the received power of the desired signal and the interfering signals from the β-th interferer, respectively. We consider MUI from two users, i.e., $i_{(1)}[n]$ and $i_{(2)}[n]$ modulated with $\mathrm{SF}_{(1)}$ and $\mathrm{SF}_{(2)}$, respectively. We also assume $|h_u| = |h_{(\beta)}| = 1$ in the following analysis. Figure 1 illustrates the FFT of three different inter-SF scenarios. In Fig. 1a and 1b, two interference signals $i_{(1)}[n]$ and $i_{(2)}[n]$ with the same power are generated by modulating with $\mathrm{SF}_{(1)} = 7$ and $\mathrm{SF}_{(2)} = 8$, respectively, and then added separately to the desired signal, which is modulated with $\mathrm{SF}_u = 9$ and without noise. This results in SIR of -16.99 dB for each case. On the other hand, in Fig. 1c, the same interference signals are superimposed on the desired signal together. In this case, the resulting SIR is -20 dB. We observe that the correct FFT bin can still be detected under both SUI scenarios. However, after superimposing the interference signals from both SFs, the original peak value is exceeded and an erroneous demodulated symbol value is obtained. From these results, it can be concluded that due to the imperfect orthogonality between different SFs, MUI can cause further degradation to LoRa demodulation performance compared to SUI. Moreover, Fig. 2 shows the symbole error rate (SER) versus SIR under noise-free condition for the perfectly synchronized desired signal with different SF combinations. For MUI, interference

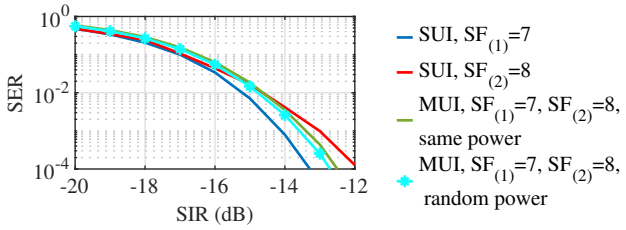

(a) MUI with different $\mathrm{SF}_{(\beta)}$.

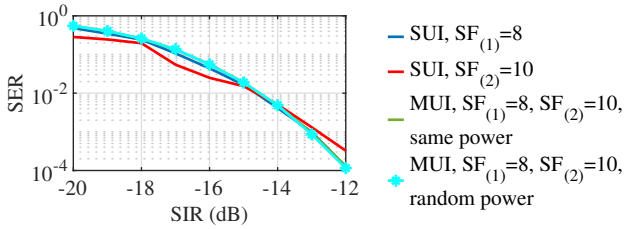

(b) MUI with different $\mathrm{SF}_{(\beta)}$.

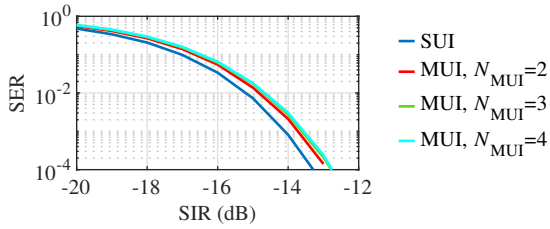

(c) MUI with the same $\mathrm{SF}_{(\beta)} = 7$ and the same power.

Fig. 2: SER results of MUI with different $\mathrm{SF}_{(\beta)}$. combinations as a function of SIR under noise-free condition, where $\mathrm{SF}_u = 9$.

signals are generated in two ways with the same and random power distribution, respectively. Note that the results of random power distribution are averaged over a sufficient number of simulations runs. We can recognize that under the same SIR, MUI results in a comparable effect on SER performance as SUI. In Fig. 2a, MUI shows slightly higher SER than both SUI conditions under $\mathrm{SIR} \leq -15$ dB and a similar curve trend can be seen in Fig. 2b in spite of the change of interference SF. Furthermore, it is also noted that MUI with different power distribution shows little difference on SER. In contrast, Fig. 2c illustrates another common scenario where MUI are modulated with the same SF with the number of interferers varying from one to four with the same power. It is evident that as the number of interferers increases, the SER also increases. Additionally, it can be observed that as the number of interferers continues to increase, the difference in the SER curve becomes less significant. Consequently, the impact of MUI cannot be neglected in LoRa, particularly under MUI, where lower power of each individual interferer than SUI is required to cause wrong demodulation.

IV. Non-aligned Inter-SF Iterative Interference Cancellation Scheme

This section introduces a method to estimate and cancel MUI iteratively without prior knowledge of the interference. In particular, we propose an algorithm to identify interference SFs and verify the presence of interference, which enables

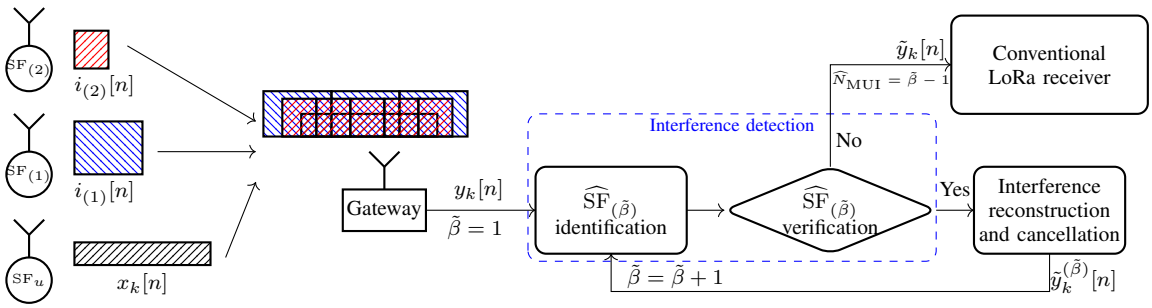

Fig. 3: Block diagram of the proposed iterative interference cancellation scheme. The desired signal is interfered with MUI with $N_{\mathrm{MUI}} = 2$. The iterative interference cancellation is performed on the received signal. The conventional demodulation is not employed until the last interference is detected.

iterative cancellation of MUI and automatic breakout. As shown in Fig. 3, we consider interference signals from multiple interferers with unknown SFs, which overlap with the signal of interest randomly. The algorithm first performs SF detection on the received signal to obtain $\widehat{\mathrm{SF}}_{(\tilde{\beta})}$, the first identified SF with index $\tilde{\beta}$. Then it verifies the presence of interference modulated with $\widehat{\mathrm{SF}}_{(\tilde{\beta})}$. If the verification result is positive, the interference signal is reconstructed and canceled using the scheme proposed in [14]. The output signal $\tilde{y}_k^{(\tilde{\beta})}[n]$ is used as the input for the next iteration of SF identification until no interference is detected. Finally, the signal $\tilde{y}_k[n]$ is sent to the LoRa demodulator. The estimated number of interferers $\widehat{N}_{\mathrm{MUI}} = \tilde{\beta} - 1$ is also obtained.

A. Interference signal SF identification with verification

The quasi-orthogonality property of LoRa signals is leveraged in [14] to propose an interference SF identification algorithm. It utilizes the fact that the DFT spectrum of a LoRa signal exhibits a prominent peak only when the correct SF is used for demodulation. It is noteworthy that even when interference signals are not aligned, resulting in two attenuated peaks in the DFT, the signal energy is still sufficiently high to detect, which allows exploiting this property for identifying the SF of interfering signals. To improve the accuracy of SF identification in the presence of noise, the peak-to-average ratio (PAR) of the DFT magnitude, rather than the peak value, is used as the metric for estimation. The PAR is defined as

$$C[N] = \frac{\left|R_N[f]\right|_{\max}}{\frac{1}{N}\sum_{f=0}^{N-1}\left|R_N[f]\right|}, \tag{6}$$

where $R_N[f]$ is the N-point DFT of the despread signal using the down chirp modulated with $\mathrm{SF} = \log_2(N)$. By looping through all possible $N \in \mathbb{T} = \{2^7, \ldots, 2^{12}\} \setminus \{2^{\mathrm{SF}_u}\}$, the identified interference SF can be obtained via $C[N]_{\max}$, which is the maximum value of $C[N]$ that corresponds to each SF. We assume that the number of available samples is sufficient to perform multiple identifications for each possible SF, where we can obtain multiple PARs from different DFT windows, selecting the largest value as $C[N]$ for output. However, false alarms may occur because the algorithm always presents an identified SF due to the loop-through mechanism, even when interference is absent.

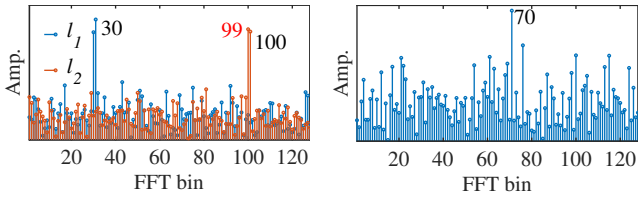

(a) Calculation of $\widehat{\delta}_l$. (b) Calculation of $\widehat{\Delta}_l$.

Fig. 4: FFT of different methods to calculate difference between $l_1 = 30$ and $l_2 = 100$ with $\mathrm{SF}_{(\beta)} = 7$ with fractional STO under AWGN.

In order to address the issue of false alarms in SF identification, a mechanism is proposed to verify the presence of interference signals based on their DFT patterns. It is important to note that even in the presence of only noise, a maximum magnitude can still be found after performing LoRa demodulation. Therefore, an additional method is needed to distinguish between noise and LoRa signals. To address this, we assume the existence of two symbols modulated with $\mathrm{SF}_{(\beta)}$ where l_1 and l_2 are the two symbol values. $N_{(\beta)} = 2^{\mathrm{SF}_{(\beta)}}$ is the symbol length and $A_{(\beta)}$ is the amplitude. We can separately obtain the decoded symbol values via conventional LoRa demodulation and calculate the difference between them as

$$\widehat{\delta}_l = (l_2 - l_1) \bmod \left(N_{(\beta)} - 1\right). \tag{7}$$

Alternatively, $\widehat{\delta}_l$ can be calculated without dechirping as described in the following. Firstly, the complex conjugate of the first signal is calculated. Multiplying it directly by the second signal, we obtain

$$s[n] = A_{(\beta)}^2 \exp\left(j\frac{2\pi\,(l_2 - l_1)\,n}{N_{(\beta)}}\right), \tag{8}$$

where the exponential terms of chirp signals are eliminated automatically. We finally obtain

$$\widehat{\Delta}_l = \arg\max_{f\in\mathbb{L}} \left|S[f]\right|, \tag{9}$$

where $S[f] = \mathcal{F}\{s[n]\}$ and $\mathbb{L} = \{0, \ldots, 2^{\mathrm{SF}_{(\beta)}} - 1\}$. It is clear that under ideal conditions or when both signals experience the same symbol shift, $\widehat{\Delta}_l$ is equal to $\widehat{\delta}_l$, which can be used as the metric to verify the presence of LoRa signals. However, when fractional sample timing offset (STO) or carrier frequency offset (CFO) are present, l_1 and l_2 can be shifted to adjacent values, resulting in $\widehat{\Delta}_l \neq \widehat{\delta}_l$. An example is shown in

Algorithm 1 Algorithm for iterative interference cancellation

Input: Received signal $y_k[n]$ with N_r samples, calibration factor ρ
Output: $\tilde{y}_k[n]$, $\widehat{N}_{\mathrm{MUI}}$

N_s samples extracted for interference detection
$\tilde{\beta} = 1$;
Verified = True;
while *Verified* = True **do**
  $\widehat{N}_{(\tilde{\beta})} \leftarrow \widehat{\mathrm{SF}}_{(\tilde{\beta})} \leftarrow$ SF Identification;
  $V_{\mathrm{DFT}} \leftarrow \mathrm{floor}(N_s/\widehat{N}_{(\tilde{\beta})})$;
  $v = 0$;
  for $b = 1 : V_{\mathrm{DFT}} - 2$ **do**
    for $D = 0 : \widehat{N}_{(\tilde{\beta})}/4 : \widehat{N}_{(\tilde{\beta})}/2$ **do**
      $r_{l1}[n] \leftarrow y_k[(b-1)\cdot \widehat{N}_{(\tilde{\beta})} + 1 + D : b \cdot \widehat{N}_{(\tilde{\beta})} + D]$;
      $r_{l2}[n] \leftarrow y_k[b \cdot \widehat{N}_{(\tilde{\beta})} + 1 + D : (b+1) \cdot \widehat{N}_{(\tilde{\beta})} + D]$;
      $l_1 \leftarrow \max|\mathrm{FFT}(r_{l_1}[n])|$;
      $l_2 \leftarrow \max|\mathrm{FFT}(r_{l_2}[n])|$;
      $\widehat{\delta_l} \leftarrow l_2 - l_1$;
      $\widehat{\Delta_l} \leftarrow \max\left|\mathrm{FFT}(r^*_{l_1}[n] * r_{l_2}[n])\right|$;
      if $|\widehat{\delta_l} - \widehat{\Delta_l}| \leq \Omega$ **then**
        $v = v + 1$;
        break
      end if
    end for
  end for
  if $v/b \geq \rho$ **then**
    $\tilde{y}_k^{(\tilde{\beta})}[n] \leftarrow$ Interference Cancellation;
    $\tilde{\beta} = \tilde{\beta} + 1$;
  else
    Verified = False; {#no interference detected}
  end if
end while
$\widehat{N}_{\mathrm{MUI}} = \tilde{\beta} - 1$;
$\tilde{y}_k[n] = \tilde{y}_k^{(\tilde{\beta})}[n]$;

Fig. 4, where the fractional STO causes the left shift of l_2 thus the wrong value of $\widehat{\delta_l}$, while the correct $\widehat{\Delta_l}$ is still obtained. Consequently, the presence of interference is verified when $\left|\widehat{\delta_l} - \widehat{\Delta_l}\right| \leq \Omega$, where $\Omega = 2$ is set as the tolerance value to compensate for the symbol shift.

B. Iterative interference cancellation

After verifying the presence of interference, interference reconstruction and cancellation are performed using the currently identified SF. We follow the segmentation method to estimate the equivalent data symbol values and signal amplitude of interference for reconstruction [14]. This approach helps mitigate the data loss caused by non-alignment and is illustrated in Fig. 5. The direct estimation of a non-aligned interfering signal with $N_{(\beta)}$ samples results in a complete loss of data information of the second signal, as it is overpowered by the first signal as shown in Fig. 5a. To overcome this limitation, we have employed a scheme where the $N_{(\beta)}$ samples are split into several distinct segments, in this example four segments as shown in Fig. 5b, and independent estimation is carried out in each segment. Each segment is treated as a complete LoRa signal modulated by an equivalent data symbol, and zero padded to ensure $N_{(\beta)}$ samples. We observe that the boundary between two consecutive signals affects only one

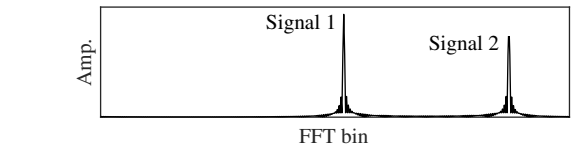

(a) FFT magnitude assuming non-aligned demodulation of two consecutive data symbols.

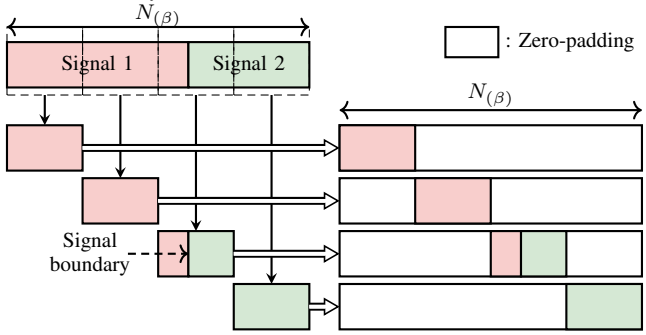

(b) The signal with length $N_{(\beta)}$ is divided into four parts with zero-padding for independent estimation.

Fig. 5: Segmentation of the interference signal.

segment, while the equivalent data symbols of other segments can be fully recovered. In the next step, the interfering signals are reconstructed and subtracted from the received signal, leading to an effective reduction of SIR. Then, the resulting signal is used for the next round of SF identification and verification until no interference is detected. Finally, after interference cancellation, the signal will be demodulated in the conventional LoRa receiver. Algorithm 1 illustrates the whole procedure. It is noted that a threshold ρ is introduced for a calibration of the SF verification, where multiple groups of verification are performed on consecutive signals. If the successful verification ratio is not lower than ρ, we can confirm that there is interference and vice versa. Additionally, in order to mitigate the influence of the non-alignment of the interference signal, the signal is shifted by $\widehat{N}_{(\tilde{\beta})}/4$ and $\widehat{N}_{(\tilde{\beta})}/2$ to perform SF verification if $|\widehat{\delta_l} - \widehat{\Delta_l}| > \Omega$.

V. Simulation Results

We employ numerical simulations to assess the efficacy of the proposed method. We conduct tests on two key components: *i*) the accuracy of interference detection, and *ii*) the accuracy of data symbol demodulation of the desired signal. Using the system model described in Section II, we simulate a LoRa transceiver chain. In every simulation iteration, we superimpose the desired signal modulated with $\mathrm{SF}_u = 9$ with several random interfering symbols from multiple inter-SF interferers, thus creating overlapped signals. Similarly to [17], we assume that the desired signal is perfectly synchronized, whereas the interference experiences random time and frequency offsets. Unless otherwise stated, we treat all interferers as having the same transmit power.

A. Performance of interference detection

In order to ensure the correct identification and verification of interference SF, the following two criteria must be satisfied:

TABLE I: Interference identification and verification accuracy under SIR $= -20$ dB and SNR $= -10$ dB, $N_s = 8192$.

ρ / $SF_{(\beta)}$	0.2	0.3	0.4	0.5	0.6	0.7	0.8	0.9
No interference	0.963	0.995	0.996	0.996	0.999	0.999	0.999	0.999
7 and 8	0.383	0.536	0.803	0.908	0.971	0.992	0.996	0.979
8 and 10	0.570	0.851	0.836	0.838	0.965	0.992	0.997	0.991
7 and 7	0.389	0.659	0.864	0.961	0.984	0.933	0.726	0.262

TABLE II: Interference identification and verification accuracy under SIR $= -20$ dB and different SNRs, $N_s = 8192$.

SNR(dB) / $SF_{(\beta)}$	-20	-17	-14	-11	-8	-5
No interference ($\rho = 0.6$)	0.999	0.999	0.999	0.999	0.999	0.999
7 and 8 ($\rho = 0.8$)	0.910	0.979	0.993	0.994	0.996	0.996
8 and 10 ($\rho = 0.8$)	0.996	0.997	0.997	0.997	0.998	0.998
7 and 7 ($\rho = 0.6$)	0.031	0.899	0.983	0.984	0.986	0.990

– All interference SFs must be detected accurately.
– The algorithm must terminate immediately when no interference is present.

Table I presents the impact of ρ on accuracy in various inter-SF scenarios and interference-free conditions under AWGN, where the signal-to-noise ratio (SNR) is -10 dB. It is noteworthy that the proposed scheme achieves high accuracy across all scenarios by selecting an appropriate value of ρ. When there is no interference, the algorithm demonstrates a perfect LoRa pattern recognition ability, as it exhibits an accuracy greater than 96.3% for all values of ρ and an error rate of only 0.1% as long as ρ is greater than 0.5. In contrast, when the interference is modulated with different SF, the best performance of the algorithm is achieved when $\rho = 0.8$, with an accuracy of approximately 99.6%. Notably, the proposed scheme is capable of distinguishing between interferers that are modulated with the same SF with the highest accuracy of 98.4% when $\rho = 0.6$ which is slightly lower than that achieved with interferers modulated with different SFs. This is due to the capture effect that a strong signal overpowers a weaker signal with the same SF, leading to a loss of information in the weaker signal.

Furthermore, Table II shows the accuracy versus SNR in various inter-SF scenarios and interference-free conditions under AWGN. The algorithm shows perfect accuracy under interference-free conditions and slight degradation of performance under low SNR when the interferers are modulated with different SFs. However, the performance of interferers modulated with the same SFs is highly sensitive to SNR, with an accuracy of only 3.1% when SNR $= -20$ dB compared to an accuracy higher than 90% in other scenarios. This indicates that the detection of inter-SF interference modulated with the same SF is more challenging than in other scenarios, as the stronger signal may capture or dominate the weaker signal, making it difficult to extract the weaker signal's information. As the SNR increases to -5 dB, the accuracy reaches 99%.

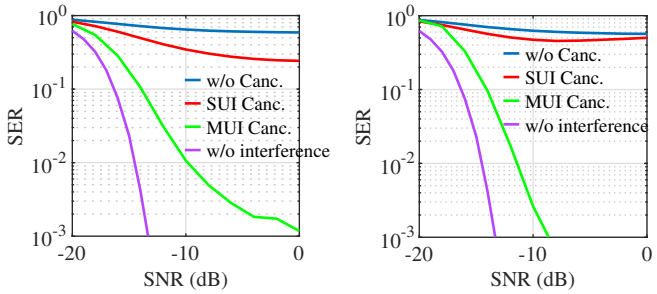

(a) $SF_{(1)} = 7$ and $SF_{(2)} = 8$. (b) $SF_{(1)} = 7$ and $SF_{(2)} = 7$.

Fig. 6: SER results of LoRa demodulation using different schemes under AWGN, SIR $= -20$ dB, $\rho = 0.6$.

B. Demodulation performance

To demonstrate the effectiveness of the proposed scheme in LoRa demodulation, we present the SER as a function of SNR in two inter-SF interference scenarios under AWGN, as shown in Fig. 6. For comparison, we also include the SER results obtained using the SUI cancellation proposed in [14], where SF identification is performed only once to cancel the interference. It is observed that the SER performance does not improve significantly when using SUI for both scenarios. Even at SNR $= 0$ dB, the SER is still above 0.5. This is because even if one SUI is accurately canceled, the remaining SUI still results in an SIR of approximately -16.99 dB, which significantly impairs the demodulation performance. On the other hand, using the proposed MUI cancellation scheme, SER performance is significantly improved. For different interference SFs, the SER is lower than 1% when SNR ≥ -10 dB and further reduces to 0.1% as SNR is higher than 0 dB. For interference modulated with the same SF, the SER is already below 0.1% when SNR is higher than -9 dB despite a lower SF identification accuracy. Furthermore, the proposed approach is analyzed under Rayleigh flat fading channel with AWGN. To ensure generalization, we assume that each channel for the desired signal and interference has an average power gain of 1, i.e., $h_u \sim \mathcal{CN}(0, 1)$ and $h_{(\beta)} \sim \mathcal{CN}(0, 1)$. Figure 7a illustrates the SER performance of different techniques in the presence MUI, where three interferers with randomly distributed power are present and result in a SIR of -15 dB. Our investigation reveals that LoRa demodulation performance is significantly impacted by the random channel gain of the Rayleigh flat fading channel. Additionally, MUI results in a constant SER of 30% at SNR levels greater than 0 dB without interference cancellation, which reduces to 17% with the SUI cancellation scheme. Our proposed MUI cancellation approach achieves an SER of less than 10% for SNR greater than -4 dB, and ultimately reaches 5% at SNR $= 20$ dB. Due to the variable channel gains and random power distribution, interference signals may fail to be identified and reconstructed at low power levels, making it challenging to achieve a further reduction in the SER even as the SNR increases. To evaluate the efficiency of the proposed interference cancellation scheme, a box plot is

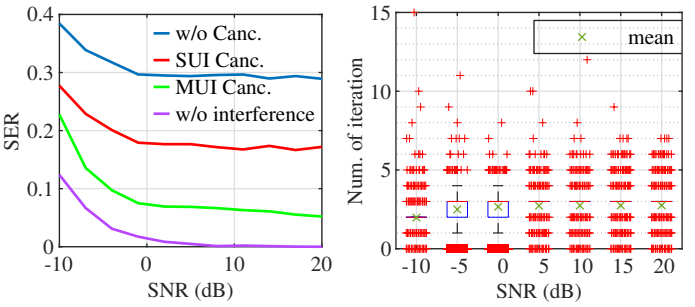

(a) SER performance.

(b) Number of iterations for interference cancellation.

Fig. 7: Performance under Rayleigh flat fading channel with three interferers modulated with $\mathrm{SF}_{(1)} = \mathrm{SF}_{(2)} = 7$ and $\mathrm{SF}_{(3)} = 8$, SIR $= -15$ dB. The power of interference is randomly distributed, $\rho = 0.6$.

generated to display the number of iterations for interference cancellation required at each SNR. As shown in Figure 7b, the minimum iteration number is 0 at each SNR, indicating that no interference was detected. The scheme achieves excellent performance, with an average iteration number ranging from 2.01 to 2.77 and a median number ranging from 2 to 3, which is close to the expected value of 3. This suggests that the scheme efficiently cancels interference. The largest outlier of 15 iterations occurred at the SNR of -15 dB, while other SNRs have outliers of 12 or less, indicating that the scheme generally performs consistently across SNRs without dead loops. The interquartile ranges (IQRs), which measure the spread of the iteration numbers, are very small at each SNR, with values of either 0 or 1. When the SNR is greater than or equal to 5 dB, the IQR is 0, indicating that the iteration numbers were highly concentrated around the median value of 3. This confirms that the scheme is precise and effective under these test conditions.

VI. Conclusion

The study demonstrates the impact of MUI on LoRa performance and proposes an iterative interference cancellation method to mitigate this issue. Our approach can concurrently detect and cancel MUI without any prior knowledge or synchronization of the interfering signals. By leveraging the patterns occurring in LoRa signals, our scheme improved demodulation performance under MUI in different channel conditions. The proposed method enables multiple devices with different SFs to transmit simultaneously, even under near-far conditions and a pure ALOHA medium access control, thus improving the scalability of LoRaWAN. The proposed technique can also improve synchronization performance by implementing it before synchronizing desired signals. Our work provides a practical and effective solution to the challenges posed by MUI in congested LoRa networks and opens up new possibilities for LoRa-based LPWAN. Furthermore, the proposed SF detection algorithm has the potential to identify consecutive upchirps, making it useful for LoRa preamble detection. For future studies, it would be valuable to explore how to adaptively select the calibration factor ρ for interference detection and cancellation of MUI from other frequency bands.

Acknowledgment

This work was funded and supported in part by the project "Industrial Radio Lab Germany (IRLG)" under contract 16KIS1010K, funded by the Federal Ministry of Education and Research, Germany.

References

[1] S. Vashi, J. Ram, J. Modi, S. Verma, and C. Prakash, "Internet of things (IoT): A vision, architectural elements, and security issues," in *2017 International Conference on I-SMAC (IoT in Social, Mobile, Analytics and Cloud) (I-SMAC)*, 2017, pp. 492–496.

[2] J. P. S. Sundaram, W. Du, and Z. Zhao, "A survey on LoRa networking: Research problems, current solutions and open issues," *IEEE Communications Surveys Tutorials*, pp. 1–1, 2019.

[3] I. B. F. de Almeida, M. Chafii, A. Nimr, and G. Fettweis, "Alternative Chirp Spread Spectrum Techniques for LPWANs," *IEEE Transactions on Green Communications and Networking*, 2021.

[4] R. Bomfin, M. Chafii, and G. Fettweis, "A novel modulation for IoT: PSK-LoRa," in *2019 IEEE 89th Vehicular Technology Conference (VTC2019-Spring)*. IEEE, 2019, pp. 1–5.

[5] B. Reynders, W. Meert, and S. Pollin, "Range and coexistence analysis of long range unlicensed communication," in *2016 23rd International Conference on Telecommunications (ICT)*, 2016, pp. 1–6.

[6] P. Maurya, A. Singh, and A. A. Kherani, "Design LoRaWAN network for unbiased communication between nodes and gateway," in *2022 14th International Conference on COMmunication Systems & NETworkS (COMSNETS)*, 2022, pp. 581–589.

[7] M. Xhonneux *et al.*, "A two-user successive interference cancellation LoRa receiver with soft-decoding," in *2021 55th Asilomar Conference on Signals, Systems, and Computers*, 2021, pp. 948–953.

[8] D. Garlisi, S. Mangione, F. Giuliano, D. Croce, G. Garbo, and I. Tinnirello, "Interference cancellation for LoRa gateways and impact on network capacity," *IEEE Access*, vol. 9, pp. 128 133–128 146, 2021.

[9] D. Croce, M. Gucciardo, S. Mangione, G. Santaromita, and I. Tinnirello, "Impact of LoRa imperfect orthogonality: Analysis of link-level performance," *IEEE Communications Letters*, vol. 22, no. 4, pp. 796–799, 2018.

[10] S. U. Minhaj, S. H. Ali, M. T. Bhatti, S. A. Hassan, A. Mahmood, and M. Gidlund, "How sic-enabled LoRa fares under imperfect orthogonality?" in *2021 International Wireless Communications and Mobile Computing (IWCMC)*, 2021, pp. 729–734.

[11] D. Croce, M. Gucciardo, S. Mangione, G. Santaromita, and I. Tinnirello, "LoRa Technology Demystified: From Link Behavior to Cell-Level Performance," *IEEE Transactions on Wireless Communications*, vol. 19, no. 2, pp. 822–834, 2020.

[12] Z. Xu *et al.*, "X-mac: Achieving high scalability via imperfect-orthogonality aware scheduling in LPWAN," in *2022 IEEE 30th International Conference on Network Protocols (ICNP)*. IEEE, 2022, pp. 1–11.

[13] S. J. Moon and W. Lee, "Friendly jamming in LoRa physical layer using imperfect orthogonality of spreading factor," in *2022 International Conference on Information Networking (ICOIN)*, 2022, pp. 423–428.

[14] Q. Zhang, I. Bizon, A. Kumar, A. B. Martinez, M. Chafii, and G. Fettweis, "A novel approach for cancelation of nonaligned inter spreading factor interference in LoRa systems," *IEEE Open Journal of the Communications Society*, vol. 3, pp. 718–728, 2022.

[15] A. Waret, M. Kaneko, A. Guitton, and N. El Rachkidy, "LoRa throughput analysis with imperfect spreading factor orthogonality," *IEEE Wireless Communications Letters*, vol. 8, no. 2, pp. 408–411, 2019.

[16] M. Chiani and A. Elzanaty, "On the LoRa Modulation for IoT: Waveform Properties and Spectral Analysis," *IEEE Internet of Things Journal*, vol. 6, no. 5, pp. 8463–8470, 2019.

[17] D. Croce, M. Gucciardo, I. Tinnirello, D. Garlisi, and S. Mangione, "Impact of spreading factor imperfect orthogonality in LoRa communications," in *Digital Communication. Towards a Smart and Secure Future Internet*, A. Piva, I. Tinnirello, and S. Morosi, Eds. Cham: Springer International Publishing, 2017, pp. 165–179.